Vehicular Channel Characterization in Orthogonal Time-Frequency Space

Thomas Blazek, Herbert Groll
Institute of Telecommunications
TU Wien
Vienna, Austria
{tblazek, hgroll}@nt.tuwien.ac.at

Stefan Pratschner
Christian Doppler Laboratory for Dependable Wireless Connectivity for the Society in Motion
TU Wien
Vienna, Austria
spratsch@nt.tuwien.ac.at

Erich Zöchmann
Department of Radio Electronics
TU Brno, Brno, Czech Republic
ezoechma@nt.tuwien.ac.at

***Abstract*—Orthogonal time-frequency space (OTFS) modulation has been suggested as modulation scheme for the fifth generation of wireless communications and beyond. The scheme is promoted as especially well apt to tackle future challenges of high mobility, millimeter wave communications (mmWave) and massive Multiple-Input Multiple-Output (MIMO). In this paper we investigate the observed channel properties in the OTFS domain from mmWave vehicular crossroads measurements. To assess the sparsity of the resulting delay-Doppler channel, we use Akaike's information criteria, which consider the trade-off between mean squared error and overfitting. Our analysis shows that in the OTFS domain, the observed channel is in deed sparse, with an optimal number of 16 channel taps out of up to 1344 possible. Our analysis furthermore shows that this property of observing sparse channels is caused mainly by the high number of orthogonal symbols resulting from modulation in two domains.**

***Index Terms*—mmWave, OTFS, Channel Characterization, V2I, Measurements**

I. Introduction

Orthogonal Time-Frequency Space (OTFS) has been promoted as a novel time-frequency-modulation format that is supposed to cope well with the challenges of future wireless networks. Its core premise is a two-dimensional modulation in the delay-Doppler domain via the Discrete Symplectic Fourier Transform (DSFT), that is then transformed into a transmit sequence [1]. There exist implementations that transmit via the Orthogonal Frequency Division Multiplexing (OFDM) domain to allow application on OFDM hardware, as well as another that transforms directly into the time domain.

This modulation has been promoted as being well suited for fifth generation communication challenges, such as massive Multiple-Input Multiple-Output (MIMO) and high mobility applications [2], [3]. The format has also been suggested for Millimeter Wave (mmWave) communication channels [4], [5]. One crucial element for the format is the characteristics and estimation of the observed channel. While channel estimation and decoding was recently studied [6], [7], few measured insights on the character of real-world channels in the OTFS domain have been published.

A. Our Contribution

In this work, we formulate measures to analyze the observed sparsity of OTFS channel responses. Sparsity based approaches were demonstrated in [8], [9]. We base our analysis on Akaike's Information Criterion [10], [11]. This allows us to find the optimum number of channel parameters for a given measurement beyond which most likely noise is being fitted. The formalism is based on our previous work in [12]–[14].

We apply the approach of [14] to vehicular 60 GHz mmWave measurements that were conducted at an urban intersection. Our analysis shows that OTFS does provide a space where the channel is considerably more sparse than the pure frequency domain. However, by introducing a normalized quality estimate, we are also able to show that this increase mainly stems from the increase in dimensionality, and not the fact that delay-Doppler domain is especially sparse for our given measurements.

B. Notation

We use boldface to denote vectors and matrices, where vectors are written as lowercase $\boldsymbol{v}$ while matrices are given as uppercase $\boldsymbol{M}$. p-norms are written as $\|\cdot\|_p$. The Hermitian transpose is denotes as $\boldsymbol{M}^H$, the Kronecker product as $\otimes$, and the column-wise vectorization of a $N \times M$ matrix into a vector of size $MN \times 1$ is denoted by the vec$(\cdot)$ function. The inverse operation is performed by unvec$(\cdot)$.

In order to enhance clarity while reading, we use t', f', τ' and ν' as *discrete-time* indices for absolute time, frequency, delay and Doppler shift. They are related to their continuous-time counterparts t, f, τ and ν via the sampling time ΔT, The subcarrier spacing ΔF, and initial time and carrier frequency T_0 and F_0:

$$t' = (t - T_0)/\Delta T \tag{1}$$

$$f' = (f - F_0)/\Delta F \tag{2}$$

$$\tau' = \tau \Delta F \tag{3}$$

$$\nu' = \nu \Delta T \tag{4}$$

II. System Model

Our goal is to estimate the sparsity and channel parameters in the OTFS domain from time-frequency traces. To achieve

this, we start out by formulating the domain transformation in a vector-matrix notation.

In general, the transformation from delay-Doppler domain to time-frequency domain is done by the DSFT. The DSFT transforms the delay-Doppler dependent scattering function S to the time-frequency dependent transfer function h via [7]

$$H[f',t'] = \frac{1}{\sqrt{DT}} \sum_{\tau'=0}^{D-1} \sum_{\nu'=0}^{T-1} S[\tau',\nu'] e^{j2\pi(t'\nu'/T - f'\tau'/D)}. \quad (5)$$

Here, T is the number of elements in the Doppler grid (and hence the number of time samples that are aggregated in one OTFS symbol). Conversely, D is the number of possible delay taps, and thus number of used subcarriers. We define the number of total elements in the grid as $N = DT$. This transform can be rewritten in matrix notation as

$$\boldsymbol{H} = \boldsymbol{F}_D^H \boldsymbol{S} \boldsymbol{F}_T. \quad (6)$$

We define $\boldsymbol{F}_D$ as the unitary discrete Fourier transform of size D. The inverse transform in this case equals

$$\boldsymbol{S} = \boldsymbol{F}_D \boldsymbol{H} \boldsymbol{F}_T^H. \quad (7)$$

We now vectorize the given transformation, and apply the identity $\mathrm{vec}(\boldsymbol{ABC}) = (\boldsymbol{C}^T \otimes \boldsymbol{A})\mathrm{vec}(\boldsymbol{B})$

$$\underbrace{\mathrm{vec}(\boldsymbol{S})}_{=\boldsymbol{s}} = \underbrace{(\boldsymbol{F}_T^H \otimes \boldsymbol{F}_D)}_{=\boldsymbol{A}_{DT\times DT}} \underbrace{\mathrm{vec}(\boldsymbol{H})}_{=\boldsymbol{h}}, \quad (8)$$

$$\boldsymbol{h} = \underbrace{(\boldsymbol{F}_T \otimes \boldsymbol{F}_D^H)}_{=\boldsymbol{A}_{DT\times DT}^{-1}} \boldsymbol{s}. \quad (9)$$

Here, the 2D-representation is calculated by applying the unvec$(\cdot)$ operation to the vectorizations.

A. Sparse Channel Estimation

We use the algorithm presented in [14] to calculate a sparse channel estimation in the delay-Doppler domain. The algorithm is based on the Complex LASSO (c-LASSO) optimization goal

$$\hat{\boldsymbol{s}}_{\mathrm{LASSO}}[t'] = \underset{\boldsymbol{s}}{\mathrm{argmin}} \left(\| (\boldsymbol{h}[t'] - \boldsymbol{A}\boldsymbol{s}) \|_2^2 + \mu \|\boldsymbol{s}\|_1 \right). \quad (10)$$

The algorithm finds an estimate that minimizes the Mean Squared Error (MSE) under the side constraint that the estimate should be sparse (enforced by the $\|\cdot\|_1$ penalty). By tuning μ, we can find an estimate with an arbitrary number of nonzero entries. This tuning can be found iteratively as described in [15].

III. Channel Characterization

We want to find a channel representation for a realization of dimension N, that uses exactly k degrees of freedom. The variable k refers to the model order. Following [12], we use the Akaike Information Criterion (AIC) as a measure to find a good trade-off between model complexity and overfitting. The criterion uses the log-likelihood function for evaluating the estimation quality, and penalizes it by the model order to avoid overfitting. For the application in this paper, this allows us to find a good estimate for the sparsity of the OTFS mmWave channel.

A. Estimation Performance Metric

In general, the AIC is defined as [10]

$$\mathrm{AIC}(\boldsymbol{h},\boldsymbol{s}) = 2k\frac{N}{N-k-1} - 2\ln(\max_{\boldsymbol{s}} f_{\boldsymbol{s}}(\boldsymbol{h})), \quad (11)$$

where $f_{\boldsymbol{s}}(\boldsymbol{h})$ is the likelihood function of $\boldsymbol{h}$ given the parametrization of $\boldsymbol{s}$. The logarithm of the likelihood function is penalized by a function that depends on the model order k. We use the refined bias that also works if $\frac{N}{k} < 40$. We assume that the LASSO estimate in (10) approximates the maximum likelihood estimate utilized in (11), that is $\hat{\boldsymbol{s}}_{\mathrm{LASSO}} \approx \mathrm{argmax}_{\boldsymbol{s}}\, f_{\boldsymbol{s}}(\boldsymbol{h})$. This behavior was observed in [12].

If this condition holds, the estimation error is unbiased and converges towards an i.i.d. complex normal distribution $e \sim \mathcal{CN}(0,\sigma^2)$ [16]. Then, the maximum likelihood and the accompanying log-likelihood is given by

$$f_{\hat{\boldsymbol{s}}}(\boldsymbol{h}) = \frac{1}{\sqrt{(2\pi)^N \det(\boldsymbol{C})}} \exp\left(-\frac{1}{2}(\boldsymbol{h}-\boldsymbol{A}\hat{\boldsymbol{s}})^H \boldsymbol{C}^{-1} (\boldsymbol{h}-\boldsymbol{A}\hat{\boldsymbol{s}}) \right),$$

$$\ln f_{\hat{\boldsymbol{s}}} = -\frac{N}{2}\ln(2\pi) - \frac{1}{2\sigma^2} \underbrace{\|\boldsymbol{h}-\boldsymbol{A}\hat{\boldsymbol{s}}\|_2^2}_{\mathrm{RSS}} - \frac{N}{2}\ln(\sigma^2), \quad (12)$$

where RSS denotes the residual sum of squares. From this, we can compute an estimated noise variance $\hat{\sigma}^2 = \frac{\mathrm{RSS}}{N}$. Then, the AIC can be written as

$$\mathrm{AIC} = 2k\frac{N}{N-k-1} + N\ln(2\pi) + \frac{N\hat{\sigma}^2}{\sigma^2} + N\ln(\sigma^2). \quad (13)$$

We now assume that we use enough samples for the noise variance estimate $\hat{\sigma}^2$ to converge towards the actual noise variance σ^2. Equation (13) simplifies to

$$\begin{aligned}\mathrm{AIC}(\boldsymbol{h},\hat{\boldsymbol{s}}) &= 2k\frac{N}{N-k-1} + N\ln(2\pi) + N + N\ln(\sigma^2)\,, \\ &= 2k\frac{N}{N-k-1} + N(\ln(2\pi)+1) + N\ln\left(\frac{RSS}{N}\right)\,. \end{aligned} \quad (14)$$

Frequently, the term $N\ln(2\pi+1)$ is dropped, as it is not dependent on k or the estimation quality, hence is not contributing to the evaluation of the optimal k. However, in this paper, we want to do evaluations also with respect to N, hence we keep the terms. When the dimensionality of our data is increased, so is the number of realizations, and hence it is more probable to find a good sparse representation. This can be seen in the last 2 terms of (14). There, as long as $\ln(\mathrm{RSS}/N) < -(\ln(2\pi)+1)$, the AIC is decreased progressively by increasing N.

We now introduce a second measure, the normalized $\mathrm{AIC}^{(n)}(\boldsymbol{h},\hat{\boldsymbol{s}})$. This is achieved by dividing the $\mathrm{AIC}(\boldsymbol{h},\hat{\boldsymbol{s}})$ by N,

$$\mathrm{AIC}^{(n)}(\boldsymbol{h},\hat{\boldsymbol{s}}) = \underbrace{\frac{2k}{N}\left(\frac{N}{N-k-1}\right)}_{\text{normalized bias}} + \underbrace{\ln(2\pi) + 1 + \ln\left(\frac{RSS}{N}\right)}_{\text{normalized likelihood}}. \quad (15)$$

We introduce this measure to specifically test for dimensionality dependence. This behavior is eliminated in the normalized AIC.

B. Akaike Weights

Based on the given formulations, we introduce the regular and normalized Akaike weights similar to [17]

$$\Phi_j = \mathrm{AIC}_j - \min_i(\mathrm{AIC}_i), \tag{16}$$

$$\Phi_j^{(n)} = \mathrm{AIC}_j^{(n)} - \min_i\left(\mathrm{AIC}_i^{(n)}\right), \tag{17}$$

$$w_j = \frac{\exp(-\Phi_j/2)}{\sum_{i=1}^{J}\exp(-\Phi_i/2)}, \tag{18}$$

$$w_j^{(n)} = \frac{\exp(-\Phi_j^{(n)}/2)}{\sum_{i=1}^{J}\exp(-\Phi_i^{(n)}/2)}. \tag{19}$$

The Akaike weights are calculated on an ensemble of measured data, and yield a number between 0 and 1 for every element of the ensemble. The closer a weight is to 1, the better fitting this element is in comparison to the competitors. In our case, we compare OTFS estimates of different sparsity and time aggregation length.

C. Measurements

Fig. 1. Image of measurement setup.

The measurements took place at an urban street crossroads as shown in Figure 1. The TX antenna is a 20 dBi conical horn antenna and mounted on a vehicle roof. The horn antenna is directed in driving direction; towards the crossroads. The RX antenna is a $\lambda/4$ monopole antenna and mounted on a crane arm, directly above the crossroads. The thereby elevated RX antenna is at a common infrastructure height of 5 m. Each measurement recording is limited to 3600 ms and starts approximately 30 m before the crossroads. The channel sounding parameters are provided in Table I. For more details regarding the measurement campaign, please refer to [18].

TABLE I
CHANNEL SOUNDING MEASUREMENT PARAMETERS

Parameter	Value
Center frequency	60.15 GHz
Subcarrier spacing	4.76 MHz
Number of subcarriers	21
Snapshot rate	178.07 μs
Delay resolution	10 ns
Recording time	3600 ms

IV. RESULTS

We calculate c-LASSO optimizations for sparseness choices of $\{4, 6, 8, 12, 16, 24\}$, and time aggregations of $T \in \{4, 8, 16, 32, 64\}$. Example results are shown in Figure 2, which demonstrates example results for one measurement run. It shows the estimated positions in delay and Doppler for all analyzed time aggregations and a sparsity of $k = 4$. Since the channel properties do not change with respect to a constant circular shift in delay domain, we shifted the delay domain such that the minimal tap delay over a measurement run equals 0. The presented traces show that a considerable amount of measurement noise for small time aggregations. Hence, the delay estimates fluctuate strongly from estimate to estimate for $T = 4$. As the time aggregation is extended, both delay and Doppler estimates become noticeably less noisy. This is caused by the effect of collecting more energy introduced by extending the estimation over a longer time block. Figure 3 shows the AIC evaluations for the presented time aggregations and chosen sparsities. The figure furthermore shows the Akaike weights calculated for each sparsity within a time aggregation. The AIC curves in the non-normalized plot appear to be straight lines, because the AIC value is dominated by the dimensionality N. Within one aggregation, only small changes are caused due to choosing different sparsities. The Akaike weights on the other hand show that for each aggregation, there is a clearly optimal sparsity choice, which can be seen by the weight w_j being close to 1. These results show us that the estimation quality is strongly dependent on the aggregation period, and that for every aggregation, we find a clear optimal choice of sparsity. However, we also want to investigate effects other than the dimensionality. Therefore, we consider the normalized AIC (Figure 4). The normalization allows us to see the dependence on the sparsity more clearly. It shows that for small aggregations, the $k = 43$ is optimal. This is a strong indicator that the measurement noise is dominating. As the time aggregation is extended, the optimal choice for k increases, however the choice stays sparse compared to the dimensionality N. The figure also shows that when normalizing with respect to the dimensionality, all the estimators produce highly similar scores. This indicates that the main gain from time aggregation comes from increased energy and dimensionality. In Figure 5, we plotted a histogram of Akaike weights computed for 4 different measurements and all listed time aggregations. The plot shows the same trend, that the non-normalized AIC tends to have clear best choices (spike

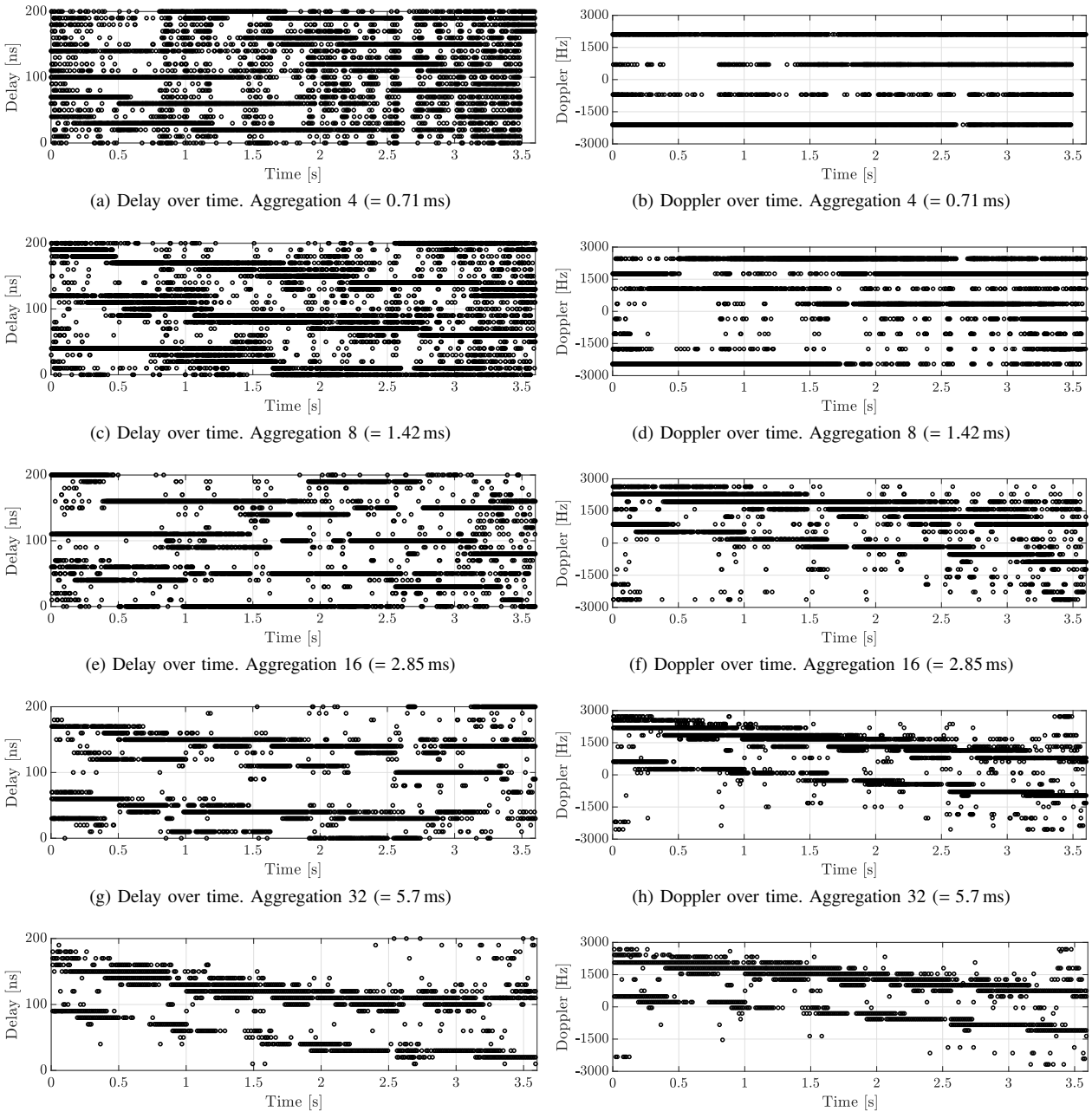

(a) Delay over time. Aggregation 4 (= 0.71 ms)

(b) Doppler over time. Aggregation 4 (= 0.71 ms)

(c) Delay over time. Aggregation 8 (= 1.42 ms)

(d) Doppler over time. Aggregation 8 (= 1.42 ms)

(e) Delay over time. Aggregation 16 (= 2.85 ms)

(f) Doppler over time. Aggregation 16 (= 2.85 ms)

(g) Delay over time. Aggregation 32 (= 5.7 ms)

(h) Doppler over time. Aggregation 32 (= 5.7 ms)

(i) Delay over time. Aggregation 64 (= 11.4 ms)

(j) Doppler over time. Aggregation 64 (= 11.4 ms)

Fig. 2. Channel estimations with Sparseness 4 and time aggregations of $T \in \{4, 8, 16, 32, 64\}$. The left plots show the positions of the delay estimates, the right plots the positions in Doppler domain. The grid is circularly shifted to avoid wraparounds in delay domain.

at 1) and clearly worse choices (large spike at 0), whereas normalization leads to a spread around 0.2. This does indicate that the larger time-frequency grid leads to strongly improved estimation qualities. However the normalized Akaike weights are all clustered at low values with no estimate being close to 1. This shows again that the optimal choice is mainly due to the large dimension, and not due to finding an inherently better matching basis.

V. Conclusions

Our results show that extending modulation into the OTFS domain does result in a channel description that is increasingly sparse compared to the total signal dimension N. However, we found that careful measures are necessary to evaluate the cause of the increased sparseness. The AIC shows us that, depending on the block length of the OTFS symbols, the channel will have ≈ 16 relevant echoes in the delay-Doppler domain. We demonstrate a great increase in estimation quality due to the time aggregation. But by normalizing the measure with respect

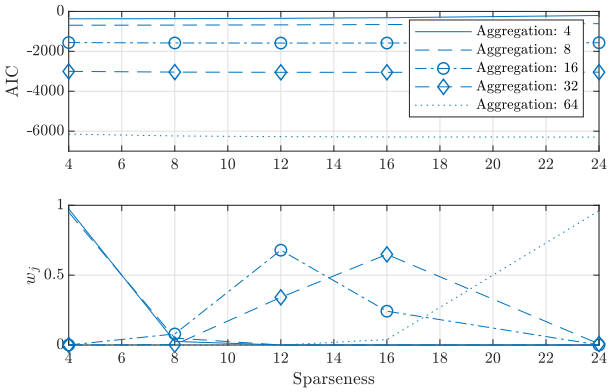

Fig. 3. Non-normalized AIC of the presented analysis.

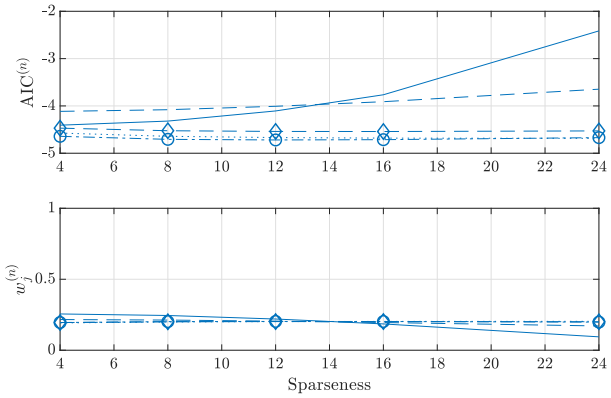

Fig. 4. $\mathrm{AIC}^{(n)}$ of the presented analysis.

to the signal dimension, we are able to show that the gain in estimation quality derives primarily from the increased signal dimension.

VI. Acknowledgments

The financial support by the Austrian Federal Ministry of Digital and Economic Affairs and the National Foundation for Research, Technology and Development is gratefully acknowledged. The research has been co-financed by the Czech Science Foundation, Project No. 17-18675S "Future transceiver techniques for the society in motion", and by the Czech Ministry of Education in the frame of the National Sustainability Program under grant LO1401.

References

[1] R. Hadani, S. Rakib, M. Tsatsanis, A. Monk, A. J. Goldsmith, A. F. Molisch, and R. Calderban, "Orthogonal Time Frequency Space Modulation," in *2017 IEEE Wireless Communications and Networking Conference (WCNC)*, March 2017, pp. 1–6.

[2] F. Wiffen, L. Sayer, M. Z. Bocus, A. Doufexi, and A. Nix, "Comparison of OTFS and OFDM in Ray Launched sub-6 GHz and mmWave Line-of-Sight Mobility Channels," in *2018 IEEE 29th Annual International Symposium on Personal, Indoor and Mobile Radio Communications (PIMRC)*, Sep. 2018, pp. 73–79.

[3] M. Kollengode Ramachandran and A. Chockalingam, "MIMO-OTFS in High-Doppler Fading Channels: Signal Detection and Channel Estimation," in *2018 IEEE GLOBECOM*, Dec 2018, pp. 206–212.

[4] R. Hadani, S. Rakib, A. F. Molisch, C. Ibars, A. Monk, M. Tsatsanis, J. Delfeld, A. Goldsmith, and R. Calderbank, "Orthogonal Time Frequency Space (OTFS) modulation for millimeter-wave communications systems," in *2017 IEEE MTT-S International Microwave Symposium (IMS)*, June 2017, pp. 681–683.

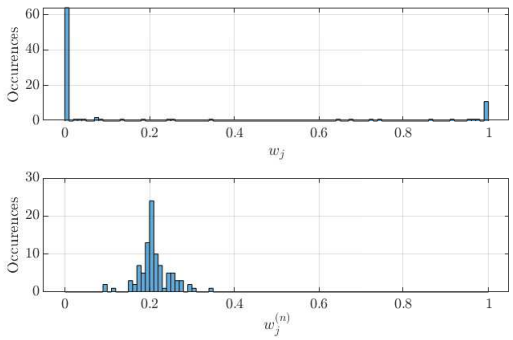

Fig. 5. Histogram of the computed Akaike weights, for non-normalized AIC (above) and normalized AIC (below).

[5] P. Raviteja, K. T. Phan, Q. Jin, Y. Hong, and E. Viterbo, "Low-complexity iterative detection for orthogonal time frequency space modulation," in *2018 IEEE Wireless Communications and Networking Conference (WCNC)*, April 2018, pp. 1–6.

[6] V. Khammammetti and S. K. Mohammed, "OTFS based Multiple-Access in High Doppler and Delay Spread Wireless Channels," *IEEE Wireless Communications Letters*, pp. 1–1, 2018.

[7] T. Zemen, M. Hofer, D. Löschenbrand, and C. Pacher, "Iterative Detection for Orthogonal Precoding in Doubly Selective Channels," in *2018 IEEE 29th Annual International Symposium on Personal, Indoor and Mobile Radio Communications (PIMRC)*, Sep. 2018, pp. 1–7.

[8] H. Groll, C. Mecklenbräuker, and P. Gerstoft, "Sparse Bayesian Learning for Directions of Arrival on an FPGA," in *2018 IEEE Statistical Signal Processing Workshop (SSP)*. IEEE, 2018, pp. 623–627.

[9] T. Blazek and C. F. Mecklenbräuker, "Sparse time-variant impulse response estimation for vehicular channels using the c-LASSO," in *Proc. of 28th Annual International Symposium on Personal, Indoor, and Mobile Radio Communications (PIMRC)*, 2018.

[10] K. P. Burnham and D. R. Anderson, "Multimodel inference: understanding AIC and BIC in model selection," *Sociological methods & research*, vol. 33, no. 2, pp. 261–304, 2004.

[11] D. Posada, T. R. Buckley, and J. Thorne, "Model Selection and Model Averaging in Phylogenetics: Advantages of Akaike Information Criterion and Bayesian Approaches Over Likelihood Ratio Tests," *Syst. Biol.*, vol. 53, no. 5, pp. 793–808, Oct 2004.

[12] T. Blazek, E. Zöchmann, and C. F. Mecklenbräuker, "Model order selection for LASSO fitted millimeter wave vehicular channel data," in *Proc. of 29th IEEE PIMRC*, Sep 2018, pp. 80–84.

[13] ——, "Approximating clustered millimeter wave vehicular channels by sparse subband fitting," in *Proc. of 29th IEEE PIMRC*, Sep 2018, pp. 91–95.

[14] ——, "Millimeter Wave Vehicular Channel Emulation: A Framework for Balancing Complexity and Accuracy," *Sensors*, vol. 18, no. 11, p. 3997, 2018.

[15] C. F. Mecklenbräuker, P. Gerstoft, and E. Zöchmann, "c–LASSO and its dual for sparse signal estimation from array data," *Signal Processing*, vol. 130, pp. 204–216, 2017.

[16] W. K. Newey and D. McFadden, "Large sample estimation and hypothesis testing," *Handbook of econometrics*, vol. 4, pp. 2111–2245, 1994.

[17] R. He, A. F. Molisch, F. Tufvesson, Z. Zhong, B. Ai, and T. Zhang, "Vehicle-to-vehicle propagation models with large vehicle obstructions," *IEEE Transactions on Intelligent Transportation Systems*, vol. 15, no. 5, pp. 2237–2248, 2014.

[18] H. Groll, E. Zöchmann, S. Pratschner, M. Lerch, D. Schützenhöfer, M. Hofer, J. Blumenstein, S. Sangodoyin, T. Zemen, A. Prokes, A. Molisch, and S. Caban, "Sparsity in the Delay-Doppler domain for measured 60 GHz Vehicle-to-Infrastructure communication channels," in *2019 IEEE International Conference on Communications (ICC)*, Shanghai, P.R. China, May 2019.